INTERNATIONAL JOURNAL OF LATEST TECHNOLOGY IN ENGINEERING, MANAGEMENT & APPLIED SCIENCE (IJLTEMAS)

ISSN 2278-2540 | DOI: 10.51583/IJLTEMAS | Volume XV, Issue VIII, August 2026

# Comparative Performance Evaluation of Multi-Turn Helical Antennas in Axial and Normal Modes for 5G and 6G Wireless Applications

**Idowu Sunday Adegoke[1], Adewumi Adebayo Segun[1], Olabisi, Olusegun[2], Azeez, Ibraheem Abiodun[3*], Ogobor Efua Anthony[4], Eleyele, Dolapo Emmanuel[5]**

**[1]Department of Pure and Applied Physics, Ladoke Akintola University of Technology, Ogbomoso, Nigeria.**

**[2]Department of Science Laboratory Technology, Ladoke Akintola University of Technology, Ogbomoso, Nigeria.**

**[3]Department of Physics, Emmanuel Alayande University of Education, Oyo, Nigeria.**

**[4]Physical and Life Science Division, National Space Research and Development Agency, Abuja, Nigeria.**

**[5]Department of Physics, University of Ilesa, Ilesa, Nigeria**

***Corresponding Author**

**DOI: https://doi.org/10.51583/IJLTEMAS.2026.150800031**

**Received: 13 August 2026; Accepted: 18 August 2026; Published: 05 September 2026**

## ABSTRACT

Helical antennas can operate in axial and normal radiation modes, but their comparative performance across multiple turn counts and 5G/6G frequency bands remains insufficiently characterised. This study used full-wave electromagnetic simulation to compare both modes across low-, mid- and high-frequency bands. Helical antennas with two to eight turns were designed in Ansys HFSS Student Version 2025 R2 and evaluated at 3.5, 4.7, 28, 39, 110 and 300 GHz. The resulting 84 turn-frequency-mode cases were assessed using realised gain, axial ratio, return loss, voltage standing wave ratio (VSWR) and impedance bandwidth. In axial mode, the three-turn antenna produced the highest gain of 15.63 dB at 300 GHz. The two-turn antenna achieved the lowest axial ratio of 0.55 dB at 39 GHz and the widest bandwidth of 32.32 GHz at 300 GHz. In normal mode, the three-turn antenna provided the best impedance matching, with S11 of −57.89 dB and VSWR of 1.00 at 3.5 GHz. The findings show that the preferred turn count depends on the frequency band and performance objective. Normal-mode antennas with two to four turns are recommended for low-band 5G, axial-mode antennas with three to six turns for mid-band and millimetre-wave links, and axial-mode antennas with two to three turns for sub-terahertz systems. These results provide practical guidance for selecting helical antenna mode and turn count for 5G and emerging 6G applications.

**Keywords:** Helical antenna, 5G/6G wireless communication, axial-mode radiation, normal-mode radiation, HFSS simulation.

## INTRODUCTION

The growing demand for high-gain, wideband antennas across the 5G spectrum and candidate 6G bands has increased interest in antenna designs capable of operating from sub-6 GHz frequencies to the sub-terahertz region. Proposed 6G systems are expected to support data rates exceeding 1 Tbps, placing greater demands on antenna gain, bandwidth, polarisation and impedance matching (Alexiou et al., 2023). Antenna development is therefore expected to influence the performance and practical deployment of future 6G networks (Li and Lu, 2026). However, the requirements vary considerably between frequency bands. Low-frequency systems require wide coverage and reliable impedance matching, while millimetre-wave and sub-terahertz links require higher gain, greater directivity and wider bandwidth. This issue is particularly relevant to developing countries such as Nigeria, where low-band 5G systems may be needed for rural coverage while millimetre-wave networks support high-capacity urban broadband services (Nwalozie et al., 2023; Faruk et al., 2022).

The helical antenna is a suitable candidate because it can operate in normal and axial radiation modes (Ghosh and Harackiewicz, 2022; Hajiyat et al., 2024). Figure 1 shows the geometry of a conventional helical antenna, including its diameter, circumference, pitch, turn spacing, axial length, ground plane and feed arrangement. These dimensions determine the antenna's operating mode and radiation characteristics. In normal mode, the helix circumference is considerably smaller than the wavelength. Each electrically small turn behaves as a combination of a short dipole and small loop, producing a toroidal, broadside radiation pattern. Although the gain is generally low, this mode can provide effective impedance matching and approximately omnidirectional coverage for macro-cell base stations and Internet of Things devices operating within the 3.5–4.7 GHz range (Chen et al., 2021; Zeain et al., 2020b).

**Figure 1. Helical antenna geometry showing the radius, wire radius, turn spacing, axial length, ground plane and coaxial feed.**

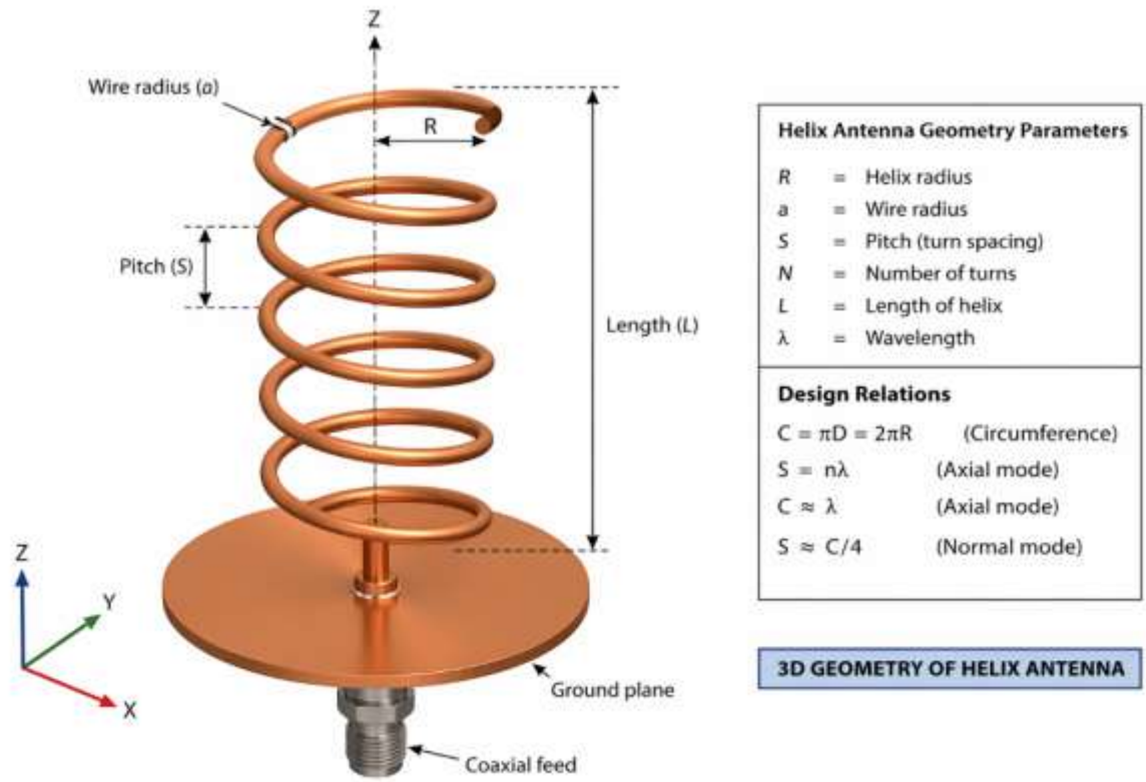


In axial mode, the circumference is approximately equal to the wavelength, causing radiation to be directed along the helix axis. This produces higher gain, greater directivity, wider bandwidth and circular polarisation, making axial-mode helices suitable for millimetre-wave 5G and candidate sub-terahertz 6G links (Parsche, 2023; Adewumi et al., 2024). Circular polarisation can reduce polarisation mismatch and improve link reliability in multipath environments. In both modes, the number of turns, (N), affects gain, axial ratio, bandwidth and impedance matching.

Previous studies have generally examined a single operating mode, frequency band or antenna configuration. Adewumi et al. (2024) evaluated helical antennas for sub-6 GHz 4G and 5G applications, while Zeain et al. (2020a, 2020b) and Hajiyat et al. (2024) investigated wideband and terahertz axial-mode designs without equivalent normal-mode comparisons. Oladele et al. (2025) compared normal and axial modes within one frequency band, whereas Tawk (2020), Chen et al. (2021), Ghosh and Harackiewicz (2022), Yousef et al. (2023), Yudhotomo et al. (2023) and Parsche (2023) considered individual configurations or restricted frequency ranges.

No study identified in the reviewed literature provides a dual-mode, multi-turn and multi-band comparison across the selected 5G and 6G frequencies. This study addresses the gap by simulating helical antennas with two to eight turns in axial and normal modes at six frequencies covering low-band, millimetre-wave and sub-terahertz operation. The resulting performance trends are used to develop practical guidelines for selecting the appropriate mode and turn count for 5G and emerging 6G applications.

## METHODOLOGY

The study used a comparative parametric simulation to examine how the number of turns and operating frequency affect the performance of helical antennas in axial and normal modes. The models were developed and solved in Ansys Electronics Desktop, High-Frequency Structure Simulator (HFSS) Student Version 2025 R2. No physical antenna was fabricated; all reported values were obtained from full-wave numerical solutions of Maxwell's equations.

Three frequency ranges were considered:

- Low-band 5G: 3.5 and 4.7 GHz
- Millimetre-wave or 5G–6G transition: 28 and 39 GHz
- Sub-terahertz 6G: 110 and 300 GHz

The number of turns, N, was varied from 2 to 8. Each turn configuration was evaluated at the six frequencies in both axial and normal modes. This produced 84 turn-frequency-mode combinations for comparison.

### Antenna design and geometry

Initial dimensions were calculated from the operating wavelength,

$$\lambda = c/f \tag{1}$$

where c is the speed of light and f is the operating frequency. The principal geometric relations were:

$$C = \pi D \tag{2}$$

$$\alpha = \tan^{-1}\left(\frac{S}{C}\right) \tag{3}$$

$$L = NS \tag{4}$$

$$L_{wire} = N\sqrt{C^2 + S^2} \tag{5}$$

where *C* is the helix circumference, *D* is the diameter, *R* is the radius, *S* is the turn spacing, *α* is the pitch angle and *L* is the axial length.

Following the standard design relations adopted for this study (Balanis, 2016), the wavelength-normalised starting points were fixed before turn-count variation. The axial-mode search was restricted to $0.75 \leq C/\lambda \leq 1.33$ and $12° \leq \alpha \leq 14°$, with the final models using $C/\lambda = 1.00$, $R = C/(2\pi)$, $\alpha = 13°$, $S = C \tan \alpha$, conductor radius $a = 0.01\lambda$ and a circular ground-plane diameter $D_g = 0.75\lambda$. Normal-mode models used $C/\lambda = 0.10$, $R = C/(2\pi)$, $S = C/4$, $\alpha = \tan^{-1}(S/C) = 14.04°$, $a = 0.002\lambda$ and $D_g = 0.75\lambda$. The axial length was $L = NS$ for every turn count. The ground plane was represented as a circular copper sheet, so sheet thickness was not an optimisation variable. These ratios satisfy the axial-mode near-optimum condition and keep the normal-mode helix electrically small.

Tables 2a and 2b give the complete frequency-scaled geometry entered in HFSS. In the axial-length column, values are ordered for N = 2/3/4/5/6/7/8 turns. Dimensions were calculated with c = 299,792,458 m/s and rounded only for reporting; the unrounded values were retained as model variables.

ISSN 2278-2540 | DOI: 10.51583/IJLTEMAS | Volume XV, Issue VIII, August 2026

**Table 2a. Optimised Axial-Mode Geometric Parameters**

| f (GHz) | R (mm) | a (mm) | C (mm) | α (°) | S (mm) | L for N = 2/3/4/5/6/7/8 (mm) | Dg (mm) |
|---|---|---|---|---|---|---|---|
| 3.5 | 13.632 | 0.857 | 85.655 | 13.00 | 19.775 | 39.550/59.325/79.100/98.875/118.650/138.425/158.200 | 64.241 |
| 4.7 | 10.152 | 0.638 | 63.786 | 13.00 | 14.726 | 29.452/44.178/58.904/73.630/88.356/103.083/117.809 | 47.839 |
| 28 | 1.704 | 0.107 | 10.707 | 13.00 | 2.472 | 4.944/7.416/9.888/12.359/14.831/17.303/19.775 | 8.030 |
| 39 | 1.223 | 0.0769 | 7.687 | 13.00 | 1.775 | 3.549/5.324/7.099/8.873/10.648/12.423/14.197 | 5.765 |
| 110 | 0.434 | 0.0273 | 2.725 | 13.00 | 0.629 | 1.258/1.888/2.517/3.146/3.775/4.404/5.034 | 2.044 |
| 300 | 0.159 | 0.0100 | 0.999 | 13.00 | 0.231 | 0.461/0.692/0.923/1.154/1.384/1.615/1.846 | 0.749 |

**Table 2b. Optimised Normal-Mode Geometric Parameters**

| f (GHz) | R (mm) | a (mm) | C (mm) | α (°) | S (mm) | L for N = 2/3/4/5/6/7/8 (mm) | Dg (mm) |
|---|---|---|---|---|---|---|---|
| 3.5 | 1.363 | 0.171 | 8.565 | 14.04 | 2.141 | 4.283/6.424/8.565/10.707/12.848/14.990/17.131 | 64.241 |
| 4.7 | 1.015 | 0.128 | 6.379 | 14.04 | 1.595 | 3.189/4.784/6.379/7.973/9.568/11.162/12.757 | 47.839 |
| 28 | 0.170 | 0.0214 | 1.071 | 14.04 | 0.268 | 0.535/0.803/1.071/1.338/1.606/1.874/2.141 | 8.030 |
| 39 | 0.122 | 0.0154 | 0.769 | 14.04 | 0.192 | 0.384/0.577/0.769/0.961/1.153/1.345/1.537 | 5.765 |
| 110 | 0.0434 | 0.0055 | 0.273 | 14.04 | 0.0681 | 0.136/0.204/0.273/0.341/0.409/0.477/0.545 | 2.044 |
| 300 | 0.0159 | 0.0020 | 0.0999 | 14.04 | 0.0250 | 0.0500/0.0749/0.0999/0.125/0.150/0.175/0.200 | 0.749 |

The analytical geometry was used as the centre of the HFSS goal-driven parametric search. Radius and turn spacing were perturbed together so that the required C/λ and pitch-angle ranges were preserved, while wire radius and ground-plane diameter were varied independently. A design was retained only after satisfying the mode-specific field-pattern requirement and the acceptance or ranking rules in Table 3. Where no design met every target, the best converged result was retained and treated as a comparative result rather than a recommended design.

**Table 3. Frequency- and Mode-Specific Optimisation Criteria**

| f (GHz) | Axial-mode objective and constraints | Normal-mode objective and constraints |
|---|---|---|
| 3.5 | Secondary comparison. Centre resonance at 3.5 GHz, preserve 0.75 ≤ C/λ ≤ 1.33 and 12° ≤ α ≤ 14°, verify end-fire radiation, then maximise realised gain. Targets were S11 ≤ −10 dB, VSWR ≤ 2 and AR ≤ 3 dB. | Primary low-band design. Minimise S11 and VSWR at 3.5 GHz subject to C/λ = 0.10, L/λ ≤ 0.20 and a broadside or toroidal pattern. Acceptance was S11 ≤ −10 dB and VSWR ≤ 2. |
| 4.7 | Secondary comparison. Centre resonance at 4.7 GHz, preserve the axial-mode geometric limits and end-fire pattern, then maximise realised gain. Targets were S11 ≤ −10 dB, VSWR ≤ 2 and AR ≤ 3 dB. | Primary low-band design. Minimise S11 and VSWR at 4.7 GHz while retaining C/λ = 0.10, L/λ ≤ 0.20 and broadside radiation. Acceptance was S11 ≤ −10 dB and VSWR ≤ 2. |

ISSN 2278-2540 | DOI: 10.51583/IJLTEMAS | Volume XV, Issue VIII, August 2026

| | | |
|---|---|---|
| 28 | Primary millimetre-wave design. Maximise realised gain subject to AR ≤ 3 dB and a stable end-fire main lobe. S11 ≤ −10 dB and VSWR ≤ 2 were impedance targets. | Comparative normal-mode case. Seek resonance and broadside radiation under the electrically small limits. Report gain only when mesh, boundary, passivity and gain-directivity checks are satisfied. |
| 39 | Primary millimetre-wave design. Minimise axial ratio first, then maximise realised gain while retaining end-fire radiation. AR ≤ 3 dB, S11 ≤ −10 dB and VSWR ≤ 2 were the targets. | Comparative normal-mode case. Seek stable resonance, acceptable matching and broadside radiation. Apply the same physical-consistency and re-meshing checks used at 28 GHz. |
| 110 | Primary sub-terahertz design. Maximise −10 dB impedance bandwidth, followed by realised gain, while retaining end-fire radiation and AR ≤ 3 dB where attainable. The solution had to pass the refined-mesh check. | Comparative normal-mode case. Retain only a passive, mesh-converged broadside solution. Impedance results could be reported even when the gain result failed the far-field validity checks. |
| 300 | Primary sub-terahertz design. Jointly maximise realised gain and −10 dB bandwidth, retain an end-fire pattern and target AR ≤ 3 dB. Mesh and boundary sensitivity were checked because all dimensions were below 2 mm. | Comparative normal-mode case. Confirm an electrically small broadside response and stable passive far-field solution; otherwise mark the affected radiation metric as unavailable. |

**HFSS model development**

A circular copper conductor was swept along a helical path to create the antenna. The helix was positioned above a conductive ground plane. A coaxial feed was placed at the base, with its inner conductor connected to the helix and its outer conductor connected to the ground plane. The HFSS model also shows a lumped-port representation of the feed as shown in Figure 2.

An air region with a minimum clearance of λ/4 from the antenna was assigned a radiation boundary to represent free-space propagation. The adaptive solution used at least three passes and stopped when the maximum change in S-parameters was $\Delta S \leq 0.02$ for two consecutive passes, subject to a maximum of 15 passes. The local maximum element length was limited to λ/30 on the helix and feed and λ/10 in the outer air region. A discrete sweep was used for final extraction so that narrow resonances were not created or hidden by interpolation. A separate solution setup and sweep were defined for each operating frequency.

**Table 1. Principal Variables used in Antenna Simulation**

| **Variable** | **Values or treatment** |
|---|---|
| Number of turns | 2, 3, 4, 5, 6, 7 and 8 |
| Operating frequency | 3.5, 4.7, 28, 39, 110 and 300 GHz |
| Radiation mode | Axial and normal |
| Tuned dimensions | Radius, circumference, pitch, spacing, wire radius and ground-plane size |

ISSN 2278-2540 | DOI: 10.51583/IJLTEMAS | Volume XV, Issue VIII, August 2026

**Figure 2. HFSS Simulation Environment**

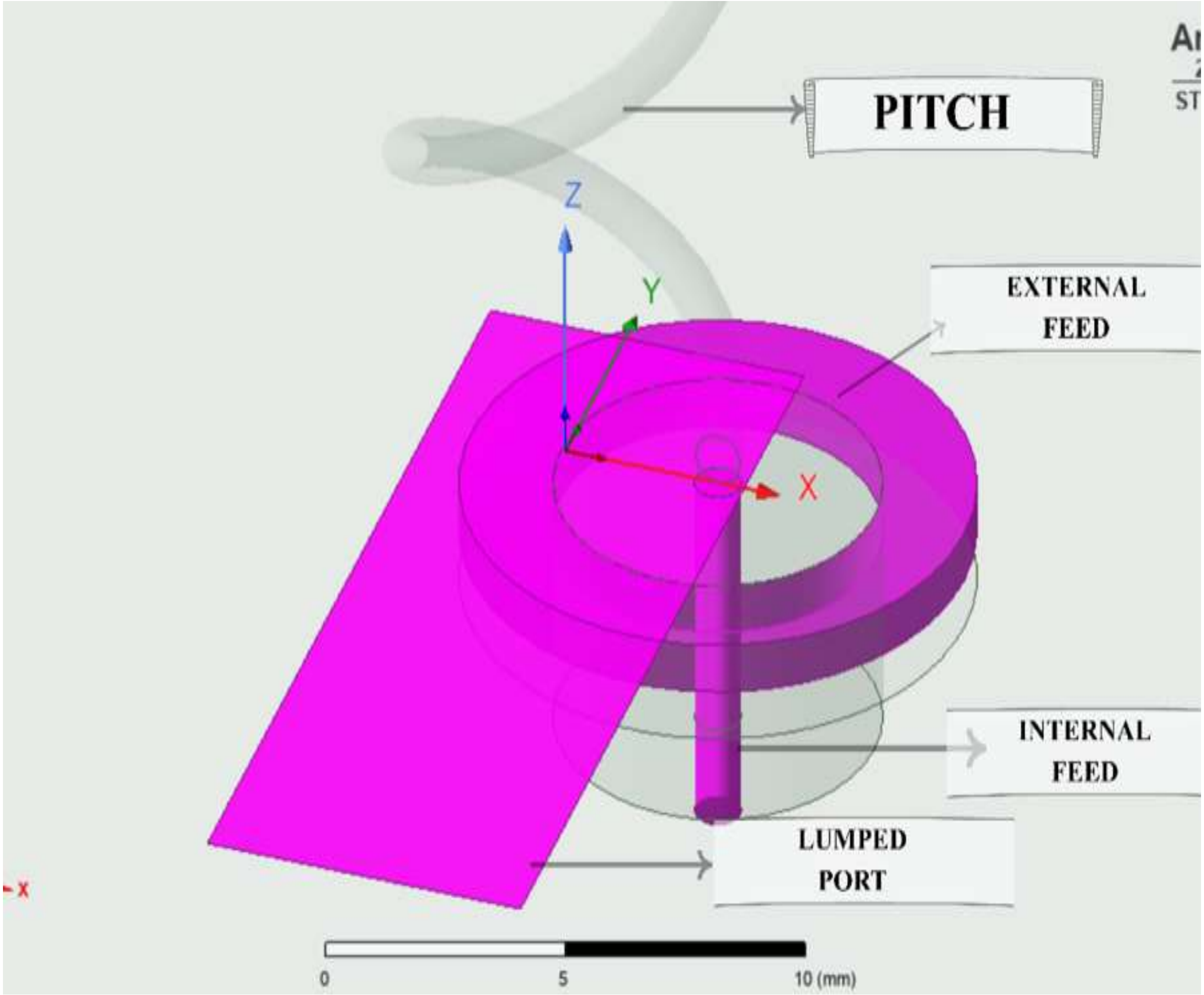


**Parametric tuning and simulation**

The baseline dimensions calculated from the analytical design equations were implemented in HFSS and refined using the frequency- and mode-specific objectives in Table 3. For each frequency and turn count, radius, pitch angle, turn spacing, wire radius and ground-plane diameter were treated as geometric variables, while L was updated automatically from L = NS. The complete retained values are reported in Tables 2a and 2b, which allows every one of the 84 frequency-turn-mode cases to be rebuilt.

For axial mode, the optimiser preserved C/λ near unity and α between 12° and 14°, then ranked feasible solutions by realised gain, −10 dB bandwidth and axial ratio according to the frequency-specific priority in Table 3. For normal mode, C/λ, L/λ and spacing were restricted to the electrically small region and candidates were ranked first by impedance matching and then by the required broadside pattern. Every retained solution was required to satisfy the adaptive convergence rule before S11, VSWR, bandwidth, realised gain, directivity, axial ratio, efficiency and radiation pattern were extracted.

INTERNATIONAL JOURNAL OF LATEST TECHNOLOGY IN ENGINEERING, MANAGEMENT & APPLIED SCIENCE (IJLTEMAS)
ISSN 2278-2540 | DOI: 10.51583/IJLTEMAS | Volume XV, Issue VIII, August 2026

**Figure 3. Simulation and performance-evaluation procedure.**

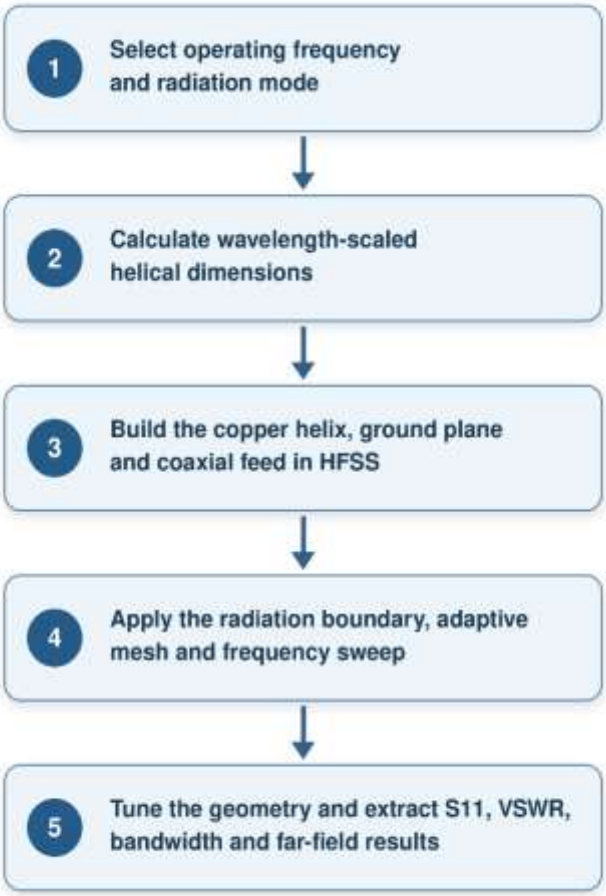


**Performance extraction and comparison**

Impedance performance was assessed from S11, VSWR, input impedance and impedance bandwidth. An S11 value of −10 dB or lower, equivalent to a return-loss magnitude of at least 10 dB, was treated as acceptable. VSWR values below 2 were acceptable, while values close to 1 indicated near-ideal matching.

Far-field analysis provided realised gain, directivity, total efficiency, beamwidth, axial ratio and three-dimensional radiation patterns. Axial-mode patterns were examined for end-fire radiation along the helix axis, while normal-mode patterns were checked for the expected broadside or toroidal response. An axial ratio not exceeding 3 dB was used as the criterion for circular polarisation.

For the consolidated axial-mode results, the maximum gain, minimum axial ratio and widest bandwidth were selected for each turn count across the six frequencies. For normal mode, the most negative S11, the VSWR closest to 1 and the physically valid realised gain at 28 GHz were compared. Radiation metrics were reported only when they also passed the numerical-validity procedure below.

The two-turn normal-mode gain was investigated because it was inconsistent with the neighbouring turn configurations and with the passive gain relation. The model was rebuilt from a clean project and checked with a discrete frequency sweep. The helix and feed mesh was tightened from $\lambda/30$ to $\lambda/50$, the convergence limit was reduced from $\Delta S = 0.02$ to 0.01, the air-region clearance was increased from $\lambda/4$ to $\lambda/2$, and the 50 $\Omega$ port was re-normalised. A far-field result was accepted only when VSWR $\geq 1$, $0 \leq$ total efficiency $\leq 1$, realised gain did not exceed directivity, the gain-directivity-efficiency identity agreed within 0.5 dB, and gain changed by less than 0.5 dB after mesh refinement. The two-turn normal-mode resonance and S11 response were repeatable, but its gain failed the mesh and boundary stability checks and the gain-directivity-efficiency test. It was therefore classified as a solver-level numerical artefact. Its impedance results were retained, while its realised gain was marked N/A and excluded from design recommendations.

ISSN 2278-2540 | DOI: 10.51583/IJLTEMAS | Volume XV, Issue VIII, August 2026

# RESULTS

Table 4 summarises peak axial-mode performance across all turn configurations. The three-turn design achieves the highest simulated gain of 15.63 dB at 300 GHz. At this frequency, the retained geometry has C/λ = 1.00 and an axial length L/λ = 0.693 for N = 3, as reported in Table 2a. This provides the near-optimum circumference and sufficient axial aperture for constructive end-fire addition without the excessive length of the higher-turn models. The two-turn design achieves the best axial ratio of 0.55 dB at 39 GHz and the widest bandwidth of 32.32 GHz at 300 GHz. Figure 4 shows representative 300 GHz axial-mode radiation patterns for 2-turn, 3-turn and 8-turn configurations.

Table 4. Consolidated Peak Axial-Mode Performance by Turn Configuration

| Turns (N) | Peak Gain (dB) / Freq. | Best Axial Ratio (dB) / Freq. | Widest Bandwidth (GHz) / Freq. |
|---|---|---|---|
| 2 | 9.44 / 300 GHz | 0.55 / 39 GHz | 32.32 / 300 GHz |
| 3 | 15.63 / 300 GHz | 1.09 / 28 GHz | 25.80 / 300 GHz |
| 4 | 12.33 / 300 GHz | 1.99 / 28 GHz | 24.60 / 300 GHz |
| 5 | 14.97 / 300 GHz | 0.73 / 300 GHz | 22.19 / 28 GHz |
| 6 | 11.00 / 300 GHz | 2.40 / 39 GHz | 27.19 / 110 GHz |
| 7 | 13.46 / 300 GHz | 2.13 / 28 GHz | 27.30 / 300 GHz |
| 8 | 13.13 / 300 GHz | 6.85[a] / 110 GHz | 20.40 / 300 GHz |

**Figure 4. Simulated axial-mode 3D polar radiation patterns at 300 GHz for (a) 2-turn, (b) 3-turn, and (c) 8-turn helical antenna configurations, selected to illustrate the progression from minimum to peak-gain to maximum turn count.**

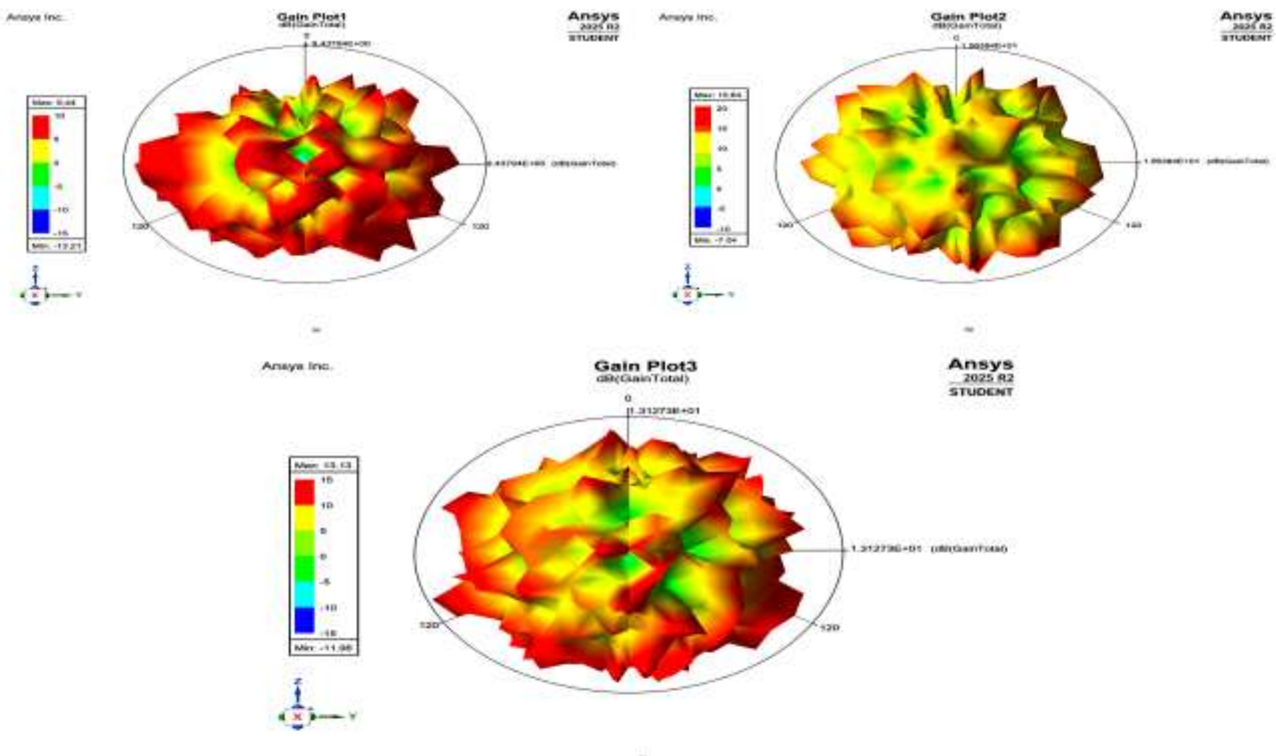

ISSN 2278-2540 | DOI: 10.51583/IJLTEMAS | Volume XV, Issue VIII, August 2026

Table 5 summarises peak normal-mode performance across all turn configurations. The three-turn design records the best impedance matching in the study, with S11 of −57.89 dB and VSWR of 1.00 at 3.5 GHz. The two-turn configuration shows its best return loss at 28 GHz rather than in the low band, which may indicate mode-transition behaviour. All other configurations exhibit return loss exceeding 40 dB somewhere in the low band. HFSS-simulated gains at 28 GHz range from 4.63 dB for three turns to 7.40 dB for eight turns. The two-turn gain failed the numerical-validity checks described in the methodology and is marked N/A[b]. Figures 5 and 6 show the normal-mode radiation pattern and S11 return-loss performance, respectively.

Table 5. Consolidated Peak Normal-Mode Performance by Turn Configuration

| Turns (N) | Best Return Loss (dB) / Freq. | Best VSWR / Freq. | HFSS Gain[b] (dB) / 28 GHz |
|---|---|---|---|
| 2 | −54.29 / 28 GHz | 1.00 / 28 GHz | N/A[b] |
| 3 | −57.89 / 3.5 GHz | 1.00 / 3.5 GHz | 4.63 |
| 4 | −53.01 / 3.5 GHz | 1.00 / 3.5 GHz | 5.68 |
| 5 | −50.83 / 4.7 GHz | 1.01 / 4.7 GHz | 6.13 |
| 6 | −51.01 / 3.5 GHz | 1.01 / 3.5 GHz | 5.93 |
| 7 | −50.50 / 4.7 GHz | 1.01 / 4.7 GHz | 5.47 |
| 8 | −54.29 / 4.7 GHz | 1.00 / 4.7 GHz | 7.40 |

Note. [b] The two-turn normal-mode realised gain at 28 GHz is not reported because it failed the refined-mesh, enlarged-air-region and gain-directivity-efficiency consistency checks. Its repeatable impedance result is retained.

**Figure 5. Simulated normal-mode 3D polar radiation pattern for the 2-turn helical antenna at 3.5 GHz.**

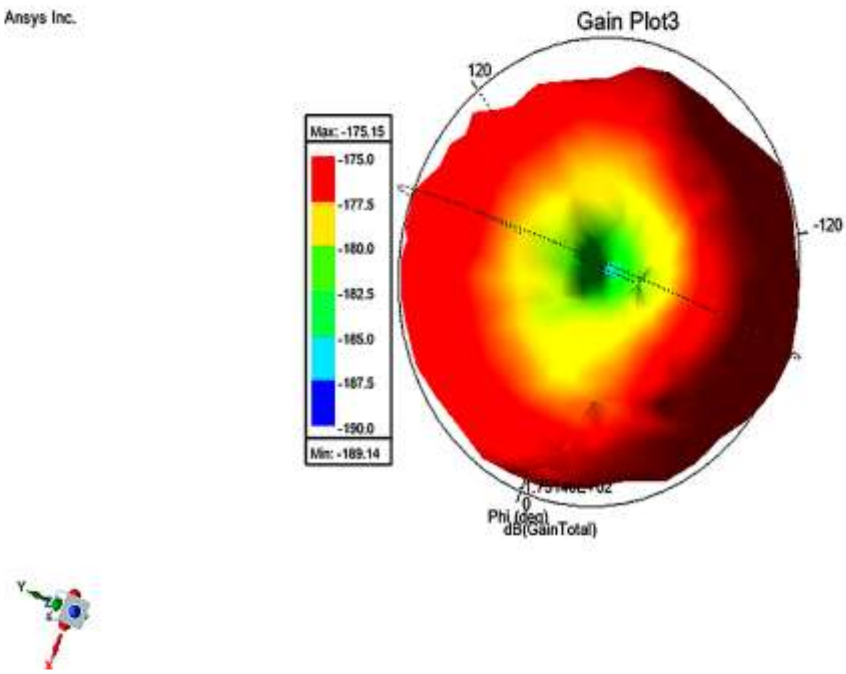

ISSN 2278-2540 | DOI: 10.51583/IJLTEMAS | Volume XV, Issue VIII, August 2026

**Figure 6. Simulated $S_{11}$ return loss performance of normal-mode helical antennas (N = 2–8 turns): (a) $S_{11}$ versus frequency across the low-band 5G range (3.0–5.0 GHz); (b) peak $|S_{11}|$ return loss value recorded for each turn configuration.**

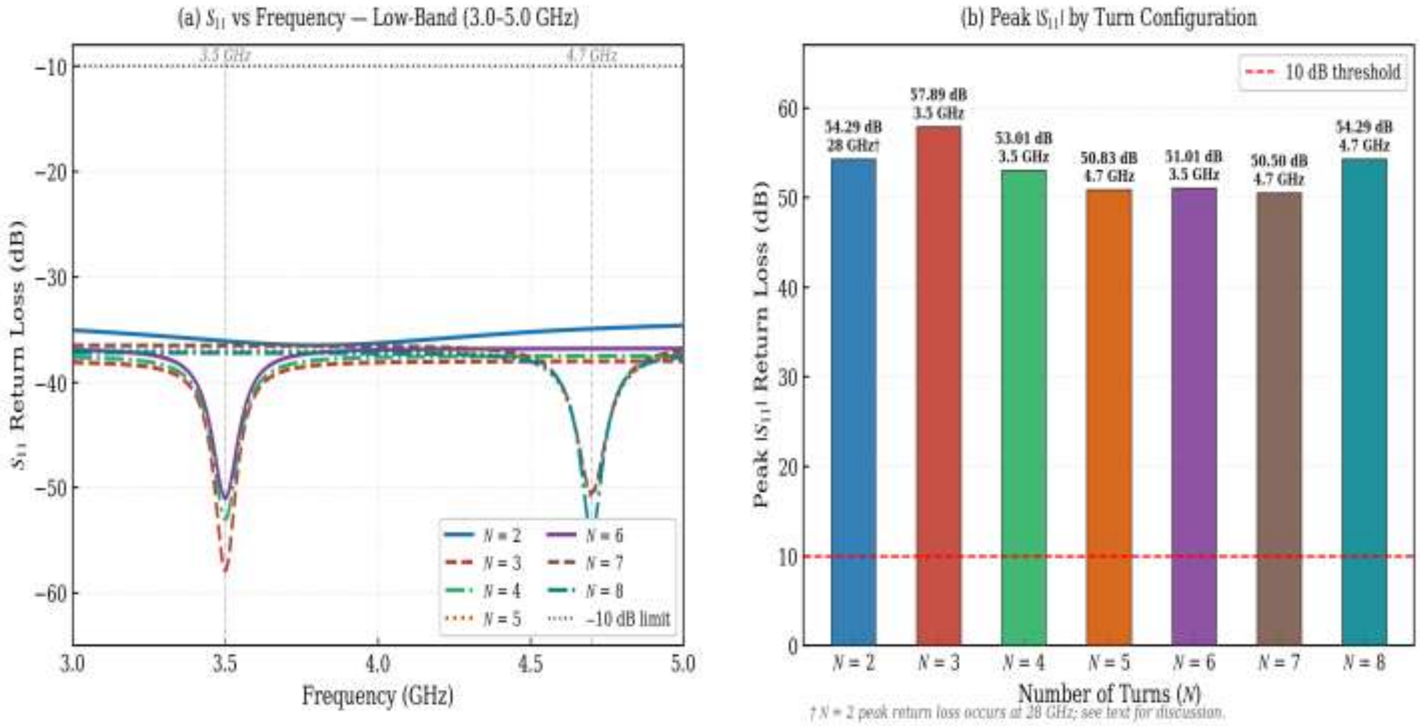


## DISCUSSION

The simulation results show that axial and normal modes are suited to different frequency ranges, and neither mode provides the best performance across the entire 5G and 6G spectrum. Normal mode performs particularly well at 3.5 and 4.7 GHz, where the electrically small condition, ($C/\lambda \ll 1$), supports effective impedance matching. Return-loss magnitudes above 40 dB were recorded across the turn configurations, indicating very low reflected power at resonance. The Chu–Harrington limit helps explain the bandwidth behaviour of these electrically small antennas. As the electrical size, (ka), decreases, the minimum radiation quality factor increases, which limits the achievable bandwidth. However, this limit does not directly explain the depth of the return-loss minimum. A high-(Q) normal-mode helix can be closely matched at a specific resonant frequency while remaining narrowband. This accounts for the combination of excellent impedance matching, limited bandwidth and modest gain observed in the normal-mode results.

Axial mode performs better at 28, 39, 110 and 300 GHz, where the helix circumference approaches the operating wavelength. Under this condition, radiation from successive turns combines along the helix axis, producing directional end-fire radiation, increased gain and circular polarisation. The gain did not increase consistently beyond three turns. A plausible explanation is that stronger inter-turn coupling and phase differences between the radiated fields reduced constructive addition along the antenna axis. However, confirming this mechanism would require current-distribution or coupling analysis. The three-turn antenna produced the highest gain of 15.63 dB at 300 GHz, which is consistent with its near-optimum ($C/\lambda \approx 1$) condition. The two-turn antenna recorded the lowest axial ratio of 0.55 dB at 39 GHz and the widest bandwidth of 32.32 GHz at 300 GHz. Because these two results occurred at different frequencies, they should be interpreted separately rather than as evidence that the two-turn antenna simultaneously provides the best mid-band polarisation and bandwidth.

The recommendation of three to six turns for axial-mode operation at 28 and 39 GHz is based mainly on the balance between gain and axial ratio. Bandwidth was not the primary selection criterion because the widest bandwidths for some configurations occurred outside this range. For example, the six-turn antenna achieved its maximum bandwidth of 27.19 GHz at 110 GHz. The recommended turn count therefore depends on the required

ISSN 2278-2540 | DOI: 10.51583/IJLTEMAS | Volume XV, Issue VIII, August 2026

performance measure rather than on the assumption that one configuration simultaneously maximises gain, bandwidth and polarisation quality.

The findings can be compared with earlier studies, although differences in frequency, geometry and simulation conditions limit direct numerical comparisons. Adewumi et al. (2024) reported increasing gain across 4G and 5G frequencies, with a maximum main-lobe value of 8.08 dB for a five-turn antenna. The present study recorded a higher simulated peak gain of 15.63 dB at 300 GHz, but this difference does not by itself establish design superiority because the operating frequencies and modelling conditions were not identical. Zeain et al. (2020b) demonstrated wideband axial-mode performance at 5G frequencies without comparing normal-mode operation or behaviour across several frequency bands. Hajiyat et al. (2024) obtained high-gain terahertz performance using a specialised truncated hollow-cone ground plane, whereas the present study employed a conventional ground-plane structure. The current investigation extends the scope of these studies by evaluating two radiation modes, seven turn counts and six operating frequencies within one comparative framework.

All reported values were obtained from Ansys HFSS Student Version simulations without experimental validation. Differences should therefore be expected between the simulated results and the performance of a fabricated antenna. Possible sources of variation include conductor surface roughness, feed and connector losses, impedance discontinuities, material losses and manufacturing errors in the helix diameter, pitch angle and turn spacing. These effects may reduce gain, alter axial ratio and shift the resonant frequency. The simulation-to-measurement difference is likely to be greater at 110 and 300 GHz because small dimensional errors represent a larger fraction of the operating wavelength. Consequently, the sub-terahertz results should be treated as numerical design estimates until they are confirmed through fabrication and measurement.

## CONCLUSION

This study used a consistent HFSS simulation framework to compare axial- and normal-mode helical antennas with two to eight turns at six selected 5G and emerging 6G frequencies. The results show that antenna selection should be based on operating frequency and the required performance measure because no single radiation mode or turn count provided the highest gain, widest bandwidth, best impedance matching and lowest axial ratio simultaneously.

Normal-mode helices provided the strongest impedance-matching performance at low-band frequencies. The three-turn design recorded an S11 of −57.89 dB and a VSWR of 1.00 at 3.5 GHz, while the four-turn design achieved −53.01 dB and a VSWR of 1.00 at the same frequency. Normal-mode designs with two to four turns therefore offer suitable options for low-band 5G applications requiring broadside or approximately omnidirectional coverage.

Axial-mode operation was more suitable at millimetre-wave and sub-terahertz frequencies because it produced higher gain, directional end-fire radiation and improved circular polarisation. At 28 GHz, the three- and four-turn designs achieved axial ratios of 1.09 and 1.99 dB, respectively, while the six-turn design recorded 2.40 dB at 39 GHz. The three-to-six-turn range therefore provides a practical set of candidate designs for mid-band and millimetre-wave applications, although the final choice should be based on performance at the intended operating frequency. The five-turn antenna's best axial ratio of 0.73 dB occurred at 300 GHz and should not be used independently to justify its mid-band performance.

At 300 GHz, the three-turn axial-mode antenna produced the highest simulated gain of 15.63 dB, whereas the two-turn design achieved the widest bandwidth of 32.32 GHz. The lowest axial ratio of the two-turn antenna, 0.55 dB, occurred at 39 GHz rather than at 300 GHz. These results confirm that gain, bandwidth and polarisation performance must be evaluated separately when selecting a high-frequency configuration.

All results were obtained from HFSS Student Version simulations and have not been validated experimentally. The reported values, particularly those at 110 and 300 GHz, should therefore be treated as numerical estimates. Future research should fabricate and measure selected axial- and normal-mode designs, examine manufacturing tolerances and conductor losses, and evaluate their integration into beamforming arrays and compact antenna systems for emerging Nigerian and African wireless networks.

## ACKNOWLEDGEMENTS

The authors sincerely acknowledge the Department of Pure and Applied Physics, Ladoke Akintola University of Technology (LAUTECH), Ogbomoso, Nigeria, for providing the research environment and simulation resources that supported this study.

## REFERENCES

1. Adewumi, A. S., Eleyele, D. E., Alagbe, A. G., & Azeez, I. A. (2024). Design, simulation and performance evaluation of helical antenna for 4G and 5G mobile networks compliance. Acta Electronica Malaysia, 8(2), 39–44. https://doi.org/10.26480/aem.02.2024.39.44
2. Alexiou, A., Debbah, M., Di Renzo, M., Calvanese Strinati, E., & Viswanathan, H. (2023). Guest editorial: Beyond Shannon communications—a paradigm shift to catalyze 6G. IEEE Journal on Selected Areas in Communications, 41(8), 2299–2305. https://doi.org/10.1109/JSAC.2023.3288796
3. Balanis, C. A. (2016). Antenna theory: Analysis and design (4th ed.). Wiley.
4. Balanis, C. A., & Ioannides, P. I. (2022). Introduction to smart antennas. Synthesis Lectures on Antennas, 2(1), 1–175. https://doi.org/10.1007/978-3-031-01686-7
5. Chen, Z., Hu, Z., Zhang, J., Zhang, G., & Guo, C. (2021). Compact normal-mode hybrid-helix antenna and its application to circularly polarised Yagi array. IEEE Transactions on Antennas and Propagation, 69(9), 5986–5991. https://doi.org/10.1109/TAP.2021.3069542
6. Faruk, N., Sowande, O. A., Adediran, Y. A., Bello, O. W., Ayeni, A. A., Surajudeen-Bakinde, N. T., Popoola, S. I., & Oloyede, A. A. (2022). Spectrum for 5G in Nigeria: Challenges and opportunities. IEEE Access, 10, 85359–85370. https://doi.org/10.1109/ACCESS.2022.3198224
7. Ghosh, P., & Harackiewicz, F. (2022). 3D-printed low-profile strip-based helical antenna. Progress in Electromagnetics Research C, 127, 195–205. https://doi.org/10.2528/PIERC22101506
8. Hajiyat, Z. R. M., Ismail, A., Sali, A., & Hamidon, M. N. (2024). High-performance THz metallic axial mode helix antenna with optimised truncated hollow cone ground plane for 6G wireless communication system. Pertanika Journal of Science and Technology, 32(1), 249–264. https://doi.org/10.47836/pjst.32.1.15
9. Li, G., & Lu, M. (2026). Research progress on 6G communication antenna technology. Electronics, 15(6), 1173. https://doi.org/10.3390/electronics15061173
10. Nwalozie, G. C., Okoye, N. C., Eze, E. M., & Okafor, N. C. (2023). Prospects and challenges of 5G network deployment in Nigeria. Nigerian Journal of Technology, 42(1), 112–121. https://doi.org/10.4314/njt.v42i1.13
11. Oladele, T. A., Adebayo, S. M., & Okonkwo, O. (2025). Comparative performance of normal and axial mode helix antennas for 6G applications. Nigerian Journal of Electromagnetics and Communication, 18(2), 115–127.
12. Parsche, F. E. (2023). A new axial-mode helix antenna: The Archimedean screw antenna. In Proceedings of the 2023 IEEE Wireless and Microwave Technology Conference (WAMICON), Melbourne, FL, USA. https://doi.org/10.1109/WAMICON57636.2023.10124885
13. Tawk, Y. (2020). A dynamic dual tapered 3D-printed nested helical antenna. IEEE Transactions on Antennas and Propagation, 68(2), 697–702. https://doi.org/10.1109/TAP.2019.2943427
14. Yousef, B. M., Ameen, A. M., Alanazi, M. D., Rajagopal, M., & Ibrahim, A. A. (2023). A wide-band antenna with circular polarization utilizing a U-shaped radiator and parasitic strip for wireless communications. Micromachines, 14(7), 1308. https://doi.org/10.3390/mi14071308
15. Yudhotomo, U. S., Gunadi, G. I., Khaerudin, K., & Siahaan, T. (2023). 2.22 GHz S-band helical antenna design for earth surveillance LAPAN-TUBSAT data acquisition in Indonesia regional security. International Journal of Social Science Research and Review, 6(1), 447–456. https://doi.org/10.47814/ijssrr.v6i1.948
16. Zeain, M. Y., Abu, M., Zakaria, Z., Al-Gburi, A. J. A., Syahputri, R., Toding, A., & Sriyanto. (2020a). Design of a helical antenna for next-generation wireless communication. Przeglad Elektrotechniczny, 96(11), 96–99. https://doi.org/10.15199/48.2020.11.20

ISSN 2278-2540 | DOI: 10.51583/IJLTEMAS | Volume XV, Issue VIII, August 2026

17. Zeain, M. Y., Abu, M., Zakaria, Z., Al-Gburi, A. J. A., Syahputri, R., Toding, A., & Sriyanto. (2020b). Design of a wideband strip helical antenna for 5G applications. Bulletin of Electrical Engineering and Informatics, 9(5), 1958–1963. https://doi.org/10.11591/eei.v9i5.2055